Improved Winding Losses Calculation based on Bessel Functions

Luo, Tianming; Niasar, Mohamad Ghaffarian; Vaessen, Peter

DOI
10.1109/TMAG.2022.3221803

Publication date
2023

Document Version
Final published version

Published in
IEEE Transactions on Magnetics

Improved Winding Losses Calculation Based on Bessel Functions

Tianming Luo[1], Mohamad Ghaffarian Niasar[1], and Peter Vaessen[1,2]

[1]Department of Electrical Sustainable Energy, Delft University of Technology, 2628 CD Delft, The Netherlands
[2]KEMA Laboratories, 6812 DE Arnhem, The Netherlands

In this article, an approach combining semi-empirical equations and the method of images is proposed for round conductor layer windings with un-gapped core. The new equation for proximity effect can convert the constant field strength from the magneto-motive force (MMF) across the core window into a frequency-dependent uniform background magnetic field strength, which can take partly the interaction between conductors into account. Geometric factors are introduced by fitting the finite element method (FEM) results to improve the accuracy. The method of images is used to calculate the field strength in order to counteract the impact of the 2-D edge effect. The new method is compared with the 2-D FEM, analytical methods, and is also validated by measurements with EE core transformers. The proposed method shows good accuracy (<10% error) compared with 2-D FEM for both high and low porosity factor windings. Therefore, it can handle more winding configurations than other 1-D analytical methods.

Index Terms—**Eddy current, losses, skin effect, transformer winding.**

I. Introduction

WINDING loss estimation is an essential part of magnetic component design. With the development of power electronics, corresponding inductors and transformers have higher power density, and heat dissipation is worse. Therefore, an accurate winding loss estimation is necessary for optimizing thermal management. Two general winding loss estimation approaches are the analytical methods and finite element method (FEM). The analytical methods are fast but are only effective for specific winding configurations due to simplification. FEM, as a general tool, can obtain accurate losses of any winding configuration. However, evaluating each configuration needs an independent simulation, which may be unfriendly to users, and another significant disadvantage is high computational effort. Therefore, the analytical approach is widely used as the first step of the design.

Most analytical methods are based on Dowell's model and Ferreira's formula [1], [2]. Dowell's model is based on the 1-D analysis for foil windings. Different shape conductors are transformed to foil conductors with equal dc conductance with the help of the porosity factor. Ferreira's formula introduced the orthogonality into the winding loss calculation and is based on the analytical solution for round conductors. Two basic methods were compared with 2-D FEM and measurements in many papers [3], [4], [5]. It is shown that Dowell's has good accuracy for compacted windings but overestimates over 30% when the porosity factor is lower than 0.6, and the skin depth is smaller than the conductor radius. Ferreira's formula leads to at least a 15% overestimation when the porosity factor is higher than 0.7 and is suit for widely spaced windings. The overestimation of Ferreira's formula was attributed to the neglect of interaction between conductors [6]. Several improvements were proposed in order to increase the effective range of the two basic methods. Whitman and Kazimierczuk [7] analyzed foil windings in the cylindrical coordinate. Nan and Sullivan [6], [8] proposed a semi-empirical equation to improve proximity effect loss estimation. Dimitrakakis et al. [9] proposed a semi-empirical model for windings with the distribution of arbitrary conductors. Bartoli et al. [10] introduced the porosity factor into Ferreira's formula, but it only works well in a certain range [3], [4]. Mühlethaler et al. [11] used Ferreira's formula and the method of images to calculate winding losses. Bahmani et al. [12] proposed a pseudo-empirical model for foil and round winding losses by fitting the FEM results. Besides, domains with homogenized complex permeability are used to replace conductors and the surrounding area in FEM to facilitate calculation [13], [14], [15].

In this article, a winding loss calculation approach, combining semi-empirical equations and the method of images, is proposed for round conductor layer windings with un-gapped cores. Like other approaches, the winding losses are separated into losses due to proximity and skin effect. The proximity effect is further separated into internal and external proximity effects, whose sources are ac currents in the other turns within the same layer and outside the layer, respectively. The new equation for external proximity effect loss considers the interaction between conductors to some degree. At the same time, a geometric factor is introduced to increase the accuracy. The new equation for the internal proximity effect is obtained through an analogy, and a geometric factor is chosen by fitting a set of 2-D FEM results. The method of images is used to determine the field applied on the winding, which counteracts the impact of the space between windings and the yoke of cores, which is called 2-D edge effect in [4].

This article is structured as follows. Section II introduces the establishment of the approach. Section III introduces the settings of simulations and samples' layout for measurement. Section IV presents a comparison between the results from the different analytical methods, FEM simulations, and the measurement of winding losses for given arrangements.

Manuscript received 2 July 2022; accepted 31 October 2022. Date of publication 14 November 2022; date of current version 23 May 2023. Corresponding author: T. Luo (e-mail: T.Luo-1@tudelft.nl).

Color versions of one or more figures in this article are available at https://doi.org/10.1109/TMAG.2022.3221803.

Digital Object Identifier 10.1109/TMAG.2022.3221803

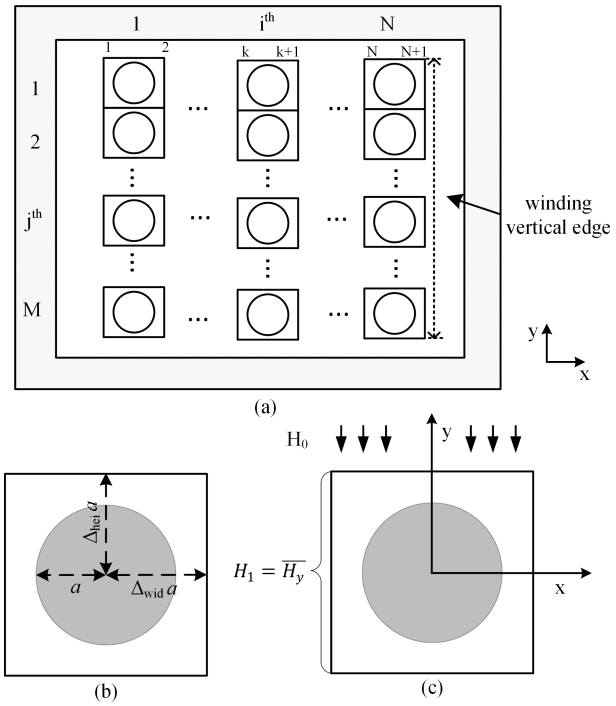

Fig. 1. (a) Geometry of a typical layer winding arrangement, (b) one cell in a winding, and (c) ideal model for the external proximity effect.

II. Model Establishment

A typical rectangular arrangement in an un-gapped core window is shown in Fig. 1(a). The core is the gray area surrounding the windings. Layers with roughly equal height are located along the x-direction, in total N layers, notation k represents the kth vertical winding edge, which is used in the magnetic field calculation in Section II-A. Each layer is wound in the y-direction and is composed of many repeated rectangle cells, M cells per layer. Cells are laid side by side, and each cell contains a single turn. A cell, as Fig. 1(b), is composed of a round conductor, with radius a, conductivity σ, and permeability μ_0, and surrounding space whose conductivity is zero and permeability is μ_0. Δ_{wid} and Δ_{hei} represent the ratio of the distance between cell edges and conductor centers in horizontal and vertical directions to the conductor radius, respectively. The fill factor can be calculated with the following equation:

$$\text{fill factor} = \pi/4\Delta_{\text{hei}}\Delta_{\text{wid}}. \tag{1}$$

Windings are excited by sinusoidal currents with angular frequency ω.

When a conductor is under a uniform background magnetic field, there is an orthogonality between the skin and proximity effects [2]. It is assumed that the winding losses per unit length in 2-D can still be calculated through proximity and skin effect losses, respectively. The proximity effect is further separated into an external proximity effect and an internal proximity effect according to the source of the field, because a layer is composed of several turns. The external proximity effect is caused by ac current in the turns of other layers. It is assumed that the x components of the field at the ends of layers are small compared with the y components and can be ignored. For the internal proximity effect, which is caused by ac current in other turns of the same layer, the magnetic field is not uniform along the x-direction. Hence, the formula from [16] cannot properly represent it. For the sake of simplicity, all the cells in one layer are assumed to have the same losses, and the losses are calculated based on a single cell, like [17].

The external proximity effect is discussed in Section II-A, magnetic field calculation is introduced in Section II-B, and the internal proximity and skin effects are discussed together in Section III-C. If there is no specific notation, all magnetic fields and currents in this article are the rms values.

A. External Proximity Effect Loss

The proximity effect formula used in [2] is derived for an isolated round conductor in a constant uniform background magnetic field with rms value H_0 [16], [18], as shown in Fig. 1(c), and its outcome is given in the following equation:

$$P_{\text{proxi}} = G_0 H_0^2$$
$$\text{with} \quad G_0 = \frac{j\pi a^2 \omega\mu_0 (J_0(\zeta_1)J_2(\zeta_2) - J_0(\zeta_2)J_2(\zeta_1))}{J_0(\zeta_2)J_0(\zeta_1)} \tag{2}$$

where G_0 is the proximity effect factor and $\zeta_1 = (1+j)a/\delta, \zeta_2 = (1-j)a/\delta$, and $\delta = (2/\omega\mu_0\sigma)^{1/2}$. J_0, J_2 are the zero and second order Bessel functions of the first kind, respectively, and δ is the skin depth.

In order to use (2), the background field H_0 needs to be calculated. In Dowell's model, the magnetic field applied to each layer can be obtained by (3), where the magnetomotive force (MMF) is determined by current and turn number, and l is the height of the core window. However, the same calculation is not correct for (2). As shown in the Appendix, the y component of the magnetic field outside the conductor is related to both coordinates and frequency. In other words, under the same uniform background field, eddy currents under different frequencies lead to different magnetic field distributions outside the conductor. The value obtained from (3) does not vary with frequency and thus cannot be regarded as the uniform background field H_0 in (2). It represents the neglect of interaction between conductors to some degree

$$H = \frac{\text{MMF}}{l}. \tag{3}$$

In order to connect the uniform background magnetic field H_0 and the constant field obtained from (3), the y component of the magnetic field H_y in an ideal situation is integrated along the vertical edge in Fig. 1(c). A new variable H_1 is calculated by the constant field obtained from (3), and the relation between H_1 and H_0 is shown in (4), details of the derivation are given in the Appendix

$$H_0 = \frac{J_0(\zeta_2)}{J_0(\zeta_2) - \frac{J_2(\zeta_2)}{\Delta_{\text{wid}}^2 + \Delta_{\text{hei}}^2}} H_1. \tag{4}$$

The value for Δ_{hei} in (4) can be easily determined by the distance between turns. However, Δ_{wid} can have an arbitrary value in the range between 1 and the distance between layers. In order to ensure that the distorted magnetic field is mainly

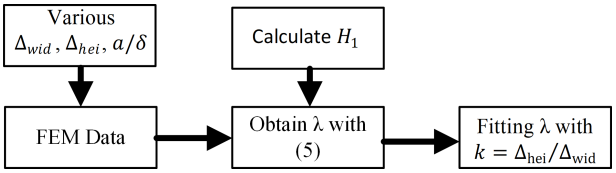

Fig. 2. Flow of fitting λ.

attributed to the eddy current in the targeted conductor, it is reasonable to set Δ_{wid} to 1. The constant MMF across the core window can be converted into a frequency-dependent uniform background magnetic field. Combining (2) and (4), external proximity loss can be calculated with the following equation:

$$P_{\text{proxi}} = GH_1^2$$
$$\text{with} \quad G = \frac{j\pi a^2 \omega \mu_0 (J_0(\zeta_1)J_2(\zeta_2) - J_0(\zeta_2)J_2(\zeta_1))}{\left(J_0(\zeta_2) - \frac{J_2(\zeta_2)}{1+\Delta_{\text{hei}}^2}\right)\left(J_0(\zeta_1) - \frac{J_2(\zeta_1)}{1+\Delta_{\text{hei}}^2}\right)}. \quad (5)$$

However, the above relation cannot fully consider the interaction between conductors. In order to compensate for the differences, a geometry-related factor is introduced. Δ_{wid} is decided by half distance between layers and $1 + \Delta_{\text{hei}}^2$ in (5) is replaced by $\lambda\Delta_{\text{hei}}^2$, where λ is the geometric factor and is obtained by fitting 2-D FEM data. The data involve 25 sets of 2-D geometries, which cover cases with Δ_{wid}, $\Delta_{\text{hei}} = 1.1$–$2.1$, and penetration ratio $a/\delta = 0.2$–20, which could cover most cases in layer windings. The model used for the simulation is presented in Section III. The flow of fitting is shown in Fig. 2, and a one-parameter exponential growth function with the variable $k = \Delta_{\text{hei}}/\Delta_{\text{wid}}$ is chosen to fit the result. The result is shown in the following equation:

$$\lambda = y_0 + \text{A}_1 \text{e}^{k/t_1} = 1.2695 + 5.46 \cdot 10^{-5} \text{e}^{k/0.15}. \quad (6)$$

As a result, the proximity effect factor G in (5) is replaced by the following equation:

$$G = \frac{j\pi a^2 \omega \mu_0 (J_0(\zeta_1)J_2(\zeta_2) - J_0(\zeta_2)J_2(\zeta_1))}{\left(J_0(\zeta_2) - \frac{J_2(\zeta_2)}{\lambda\Delta_{\text{hei}}^2}\right)\left(J_0(\zeta_1) - \frac{J_2(\zeta_1)}{\lambda\Delta_{\text{hei}}^2}\right)}. \quad (7)$$

B. Magnetic Field Strength Calculation

Generally, windings cannot fully occupy the entire height of the core window because of the existence of bobbin and/or insulation. In order to compensate for its impact on winding loss estimation, the field strength H_1 is obtained by MMF crossing the vertical winding edges rather than crossing the whole core window, as shown in Fig. 1(a). Although the value is changed under different frequencies, it does not change significantly due to the relatively small radius and small gap compared with the layer height. Therefore, it is assumed that the MMF across the vertical winding edges does not change with frequency. The method of images is used to obtain the field strength H_1 [19]. For simplification, the magnetic core is assumed to be ideal, and permeability is infinite, $k_i = 1$, and internal reflection due to the finite thickness of the core is negligible.

The four edges of the magnetic core are symmetry axes, and the more layers of image current are used, the more accurate

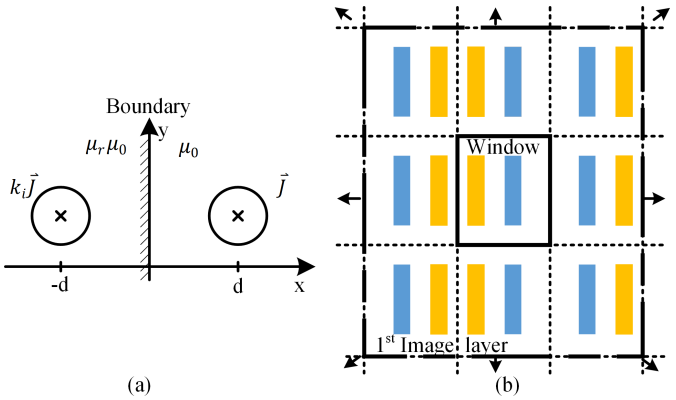

Fig. 3. Illustration of the method of images. (a) Basic idea. (b) Method applied to winding window.

the result is, as shown in Fig. 3(b). Because the MMF cross the vertical winding edges is assumed to keep constant under varying frequencies, the field strength H_1 is calculated under the dc situation.

The magnetic field H_1 applied on each layer is calculated according to the following steps.

1) Generate several layers of image conductors, like Fig. 3(b), and calculate conductors' Cartesian coordinates x_{ijn} and y_{ijn}. Note ij represents the source of a series of conductors, which is the jth conductor in ith layer, and n is the nth conductor in the series of ij conductor. Each real conductor would generate a series of conductors, including all its image conductors and itself.
2) Calculate ΔF_{kijn} of each conductor and winding vertical edge in Fig. 1(a), which is the MMF caused by the nth conductor in ij series of conductors along the kth edge. It is obtained by the integral of the magnetic field H_y over layers' height h_{layer}, as follows:

$$H_y = \frac{I(x - x_{ijn})}{2\pi\left((x - x_{ijn})^2 + (y - y_{ijn})^2\right)} \quad (8)$$
$$\Delta F_{kijn} = \int_{h_{\text{layer}}} H_y dy = \frac{I}{2\pi} \arctan\left(\frac{y - y_{ijn}}{x_k - x_{ijn}}\right)\Bigg|_{y_{k-}}^{y_{k+}}. \quad (9)$$

3) Calculate the average field strength H_k on kth edge

$$H_k = \sum_{i=1}^{N}\sum_{j=1}^{M}\sum_{n}\frac{F_{kijn}}{h_{\text{layer}}}. \quad (10)$$

4) The value H_{1i} used in (5) for ith layer is the average on both two vertical edges of one layer [8]

$$H_{1i} = \frac{H_k + H_{k+1}}{2}. \quad (11)$$

C. Skin and Internal Proximity Effect Losses

Skin effect losses are generally represented by (12), where F_{ac} is the skin effect factor, R_{dc} is the dc resistance, and I is

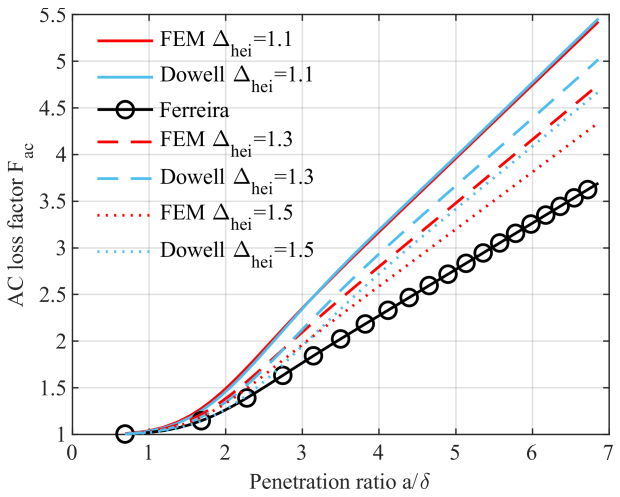

Fig. 4. AC loss factors obtained from FEM simulation, Dowell's model, and Ferreira's formula in cases where $\Delta_{\text{hei}} = 1.1, 1.3, 1.5$.

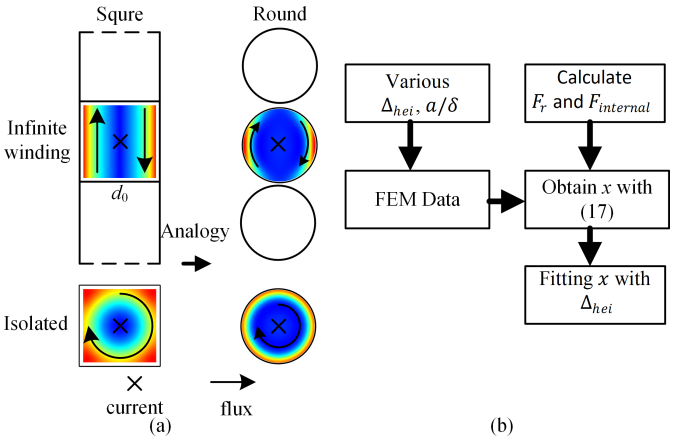

Fig. 5. Illustration of (a) analogy between square conductors and round conductors and color represents current density (b) flow of fitting x.

the current flowing through the conductor

$$P_{\text{skin}} = F_{\text{ac}} R_{\text{dc}} I^2. \tag{12}$$

Fig. 4 shows the comparison between the ac losses factor for an infinite long layer consisting of round conductors from FEM simulations and the other two methods. It is obvious that Ferreira's formula underestimates losses, and with factor Δ_{hei} increasing, i.e., winding arrangement becoming sparser, the results become better. Dowell's model performs well when Δ_{hei} is small, i.e., the porosity factor is small.

Although Ferreira's formula is the exact solution for skin effect loss in round conductors, the ac losses factor here includes not only skin effect losses but also the internal proximity effect losses, which is caused by ac currents in other turns of the same layer. It explains the difference between FEM and Ferreira's results. Dowell's model shows better results because if an infinite long foil is regarded as an infinite long layer composed of square conductors, the internal proximity effect is already included. The porosity factor can partly compensate for the difference between foil and round windings, and with factor Δ_{hei} increasing, there would be more error.

It is hard to find an exact solution for the internal proximity effect, because the induced magnetic field by other turns is not uniform. However, the solutions for an isolated square conductor and an infinite long layer of square conductors, i.e., foil, are already derived in references, and an analogy can be introduced for round conductors, as shown in Fig. 5(a).

Stoll analyzed the isolated 2-D conductor assuming the same tangential magnetic field strength on the surface [20], which only involves skin effect. Its skin effect factor in square conductors can be calculated with the following equation, where d_0 is the side of a square conductor

$$F_{\text{squ}} = \frac{1}{2} + \frac{d_0}{4\delta} \frac{\sinh(d_0/\delta) + \sin(d_0/\delta)}{\cosh(d_0/\delta) - \cos(d_0/\delta)}. \tag{13}$$

In Dowell's model, the skin effect factor for a foil was derived as (14), which can also be regarded as a layer composed of the same square conductors

$$F_{\text{Dowell}} = \frac{d_0}{2\delta} \frac{\sinh(d_0/\delta) + \sin(d_0/\delta)}{\cosh(d_0/\delta) - \cos(d_0/\delta)}. \tag{14}$$

The skin effect factor for isolated round conductors is given in (15), which has a similar form as (13). Equation (16) is obtained by analogy with the difference between (13) and (14), and it is regarded as an approximation of ac losses factor of a round conductor layer excepting the skin effect part

$$F_{\text{r}} = \frac{1}{2} + \frac{1}{2}\text{real}\left(\frac{J_0(\zeta_2) - J_2(\zeta_2)}{J_0(\zeta_2) + J_2(\zeta_2)}\right) \tag{15}$$

$$F_{\text{internal}} = \frac{1}{2}\text{real}\left(\frac{J_0(\zeta_2) - J_2(\zeta_2)}{J_0(\zeta_2) + J_2(\zeta_2)}\right) - \frac{1}{2}. \tag{16}$$

Because the losses factor in (16) is for the case without a gap between turns, and the magnetic field due to other turns varies with different distances between turns, a geometric factor x is introduced, and the ac losses factor of a round conductor layer becomes

$$F_{\text{layer}} = F_{\text{r}} + x F_{\text{internal}}. \tag{17}$$

The value of factor x is obtained by the curve fitting of 2-D FEM data, which covers cases with $\Delta_{\text{hei}} = 1.1$–$2.1$, and penetration ratio $a/\delta = 0.2$–20. The details of the simulation are shown in Section III. The internal proximity effect is related to the distance between turns. Therefore, Δ_{hei} is chosen as the variable. In order to keep the value around 1 when $\Delta_{\text{hei}} = 1$, and the value is 0 when $\Delta_{\text{hei}} = \infty$, a rational function is chosen, and the approximation of the factor x is given by

$$x = \frac{0.9223}{\Delta_{\text{hei}}^{3.424}}. \tag{18}$$

After fitting, losses from (7) and (18) are compared with corresponding FEM data. The quality of the fit is shown in Table I.

The gap between core yoke and winding also influences the internal proximity effect. Equation (17) is based on the infinite long layer with round conductors. It means there is always a couple of turns having the same distance and opposite

TABLE I
QUALITY OF THE FIT

Loss source	Chi-square	R^2	NRMSE
External proximity effect (7)	0.0462	0.9928	0.9153
Skin and internal proximity effect (18)	0.0013	0.9989	0.9662

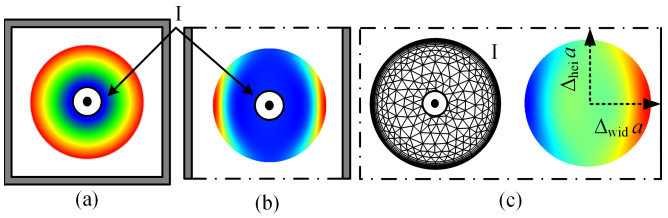

Fig. 6. Illustration of model setting, (a) skin effect losses of a conductor, (b) eddy current losses in an infinite long layer, and (c) external proximity effect, and color represents current density.

position referring to a certain turn. However, if there is a gap, some turns do not have corresponding turns at opposite positions referring to a certain turn. It leads to a larger field presenting on the referred turn, especially for the end of the layer. Therefore, when the gap height is comparable to or even larger than the layer height, (17) would lead to a considerable error. In this article, the windings' height is assumed to be much larger than the gap height, and the error of (17) is acceptable.

III. SIMULATION SETTING AND SAMPLE LAYOUT

In order to acquire geometric factors and provide a reference, 2-D FEM simulations were performed. The COMSOL software was used for all simulations.

For curve fitting purposes, the models would contain one or two cells with different boundary conditions for different effects, shown in Fig. 6.

1) For skin and internal proximity effect losses, one cell was used, as Fig. 6(a) and (b). The round conductor is set as a coil with a certain current. A magnetic material (gray domain) of relative permeability $\mu_r = 2200 \gg 1$ surrounds the rectangle cell. Using a magnetic core rather than a large air space is to consider the potential impact of the existence of core on skin effect loss. In Fig. 6(b), dot-dashed lines were set as perfect magnetic conductors, which can be seen as even symmetry axes. The gray domain is set as an infinite element domain with air properties. Then, it is set as magnetic material with a high relative permeability to simulate the potential impact of the core on eddy current losses.
2) For the external proximity effect, two cells were used, as shown in Fig. 6(c). Both were set as coils, the net current in the right-side conductor was set as zero, and another was set as a certain value to produce a magnetic field. Three dot-dashes boundaries of the model were set as perfect magnetic conductors, and the other one was magnetic insulation to simulate an ideal core and keep the magnetic flux closed. The two cells model can reproduce the uneven magnetic field distribution under low frequency and the interaction between the source and target conductor.

TABLE II
INFORMATION ABOUT DUT

Sample	DUT1	DUT2
Conductor Diameter	1mm	0.8mm
Core window	30.4mm*9mm	
Windings height	26.1mm	
Winding arrangement (from inside to outside)	23+22:22+23	12×2:12
Δ_{hei}	0.135 for 23 turns 0.186 for 22 turns	1.72
Δ_{wid}	≈0.27	≈2.29
Porosity factor	0.67 for 23 turns 0.64 for 22 turns	0.28
DC resistance	1st winding 0.078Ω 2nd winding 0.092Ω	1st winding 0.075Ω 2nd winding 0.044Ω
The mean turn length (MTL)	88.16 mm	97.62 mm

There are three variables for curve fitting purposes: frequency, Δ_{wid}, and Δ_{hei}. The parameter settings for fit were already mentioned previously. Boundary layer mesh is used to guarantee simulation accuracy, as shown in Fig. 6(c).

Next, two transformers with un-gapped cores were built with different Δ_{hei} and Δ_{wid}. The cores used are TDK N87 EE 42/21/20. The coil former results in a gap between windings and core yoke, 2.15 mm on each side. Δ_{hei} was roughly controlled by the thickness of the insulation layer of wires and calculated by the height of windings over the number of turns. Basic information about the devices under test (DUT) is given in Table II. DUT1 represents compacted winding, which has two layers for each side, and DUT2 represents winding with a low porosity factor, which has two layers for the primary side and one layer for the secondary side.

The simulation for winding losses per unit length in core window is built based on the layout in Table II. The corresponding penetration ratio a/δ varied from 0.6 to 6.8.

IV. RESULT AND COMPARISON

In this section, results from different methods, 2-D FEM simulation, and measurement are compared.

A. Skin and Internal Proximity Effect Losses

As described in Section II-B, when there is a winding layer composed of round conductors, the eddy current loss is caused by the skin effect and the internal proximity effect. This section compares the losses of a single round conductor and one in a layer surrounded by a core between FEM simulations and different analytical methods.

Fig. 7(a) shows the relative error of Ferreira's formula for a single conductor in a core compared with simulation results when the penetration ratio is 2. When $\Delta_{wid} = \Delta_{hei}$, differences between FEM and Ferreira's formula are close to 0%, which is also reported in [17]. In the most different case, i.e., the difference between Δ_{wid} and Δ_{hei} is the biggest, and the relative error is lower than 5%. In most cases, the core window is much larger than one turn's cross section area, and the impact of the core can then be neglected. Therefore, the formula for skin effect is accurate enough.

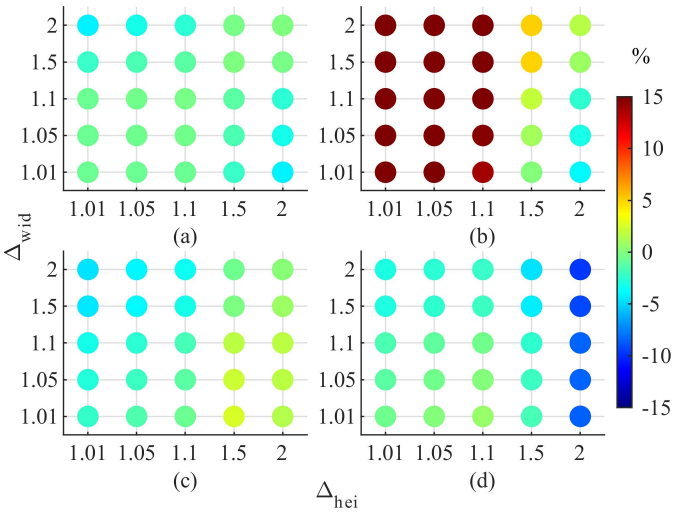

Fig. 7. Relative difference% between (a) Ferreira's formula and FEM for a single conductor, (b) FEM for a winding layer and a single conductor, (c) new equation and FEM for a winding layer, and (d) Dowell's model and FEM for a winding layer, penetration ratio a/δ used is 2.

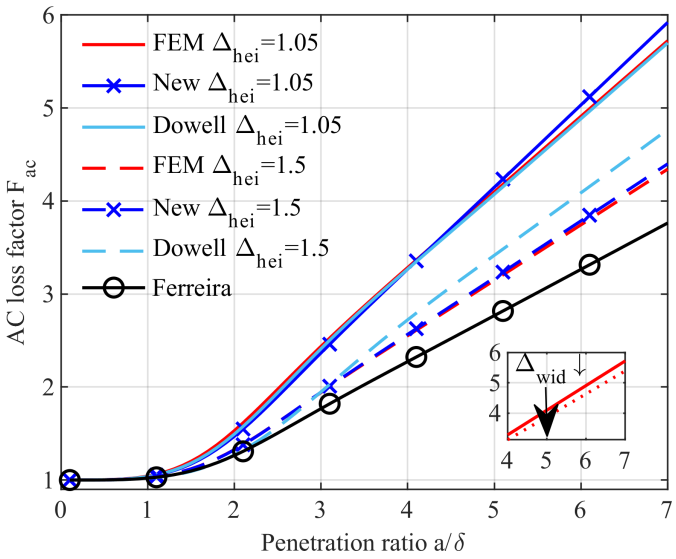

Fig. 8. AC loss factors of skin and internal proximity effect from the FEM simulation, Dowell's model, the new equation, and Ferreira formula, when Δ_{hei} is 1.05 and 1.5, respectively, and Δ_{wid} is 1.5. Inset: Factors from the FEM simulation when Δ_{hei} is 1.05, and Δ_{wid} is 1.05 and 0.5, respectively.

Fig. 7(b) shows the difference between the losses of a single conductor and one in a layer, and it is obvious that the smaller Δ_{hei}, the heavier the impact between turns is. Fig. 7(c) and (d) compares the new equation and Dowell's model with FEM results for different geometries when the penetration ratio is 2. In general, the new equation shows a minor error compared with others. It gives a slightly larger error when turns are close. This is because the equation obtained through analogy can only give approximate eddy current losses due to the internal proximity effect, and the geometric factor x is not related to frequency. For Dowell's model, with increasing Δ_{hei}, errors become more significant. It is attributed to the smaller porosity factor, and it cannot compensate for the difference between the model and real cases.

Fig. 8 shows the ac loss factor under varying penetration ratios, when Δ_{hei} is 1.1 and 1.5, respectively, and Δ_{wid} is constant at 1.5. The new equation can better follow the FEM curves compared with other methods. The new equation shows a similar result as Dowell's model when Δ_{hei} is 1.1, and more accurate results when Δ_{hei} is 1.5. The inset figure shows the impact of core, i.e., the ac loss factor becomes smaller with smaller Δ_{wid}. In general, a layer can only be close to one side of the core, and there is always some distance between windings and core. Therefore, the impact of the core can be ignored.

Although the winding loss error due to this part may not be significant for multilayer transformers, the new equation could be helpful for windings with few layers.

B. External Proximity Effect Loss

Compared with the skin effect, the proximity effect loss attracts more attention, and several improved methods were proposed. In this section, the FEM results are compared with (4), (6), two classic methods, and Nan's improved equation [8].

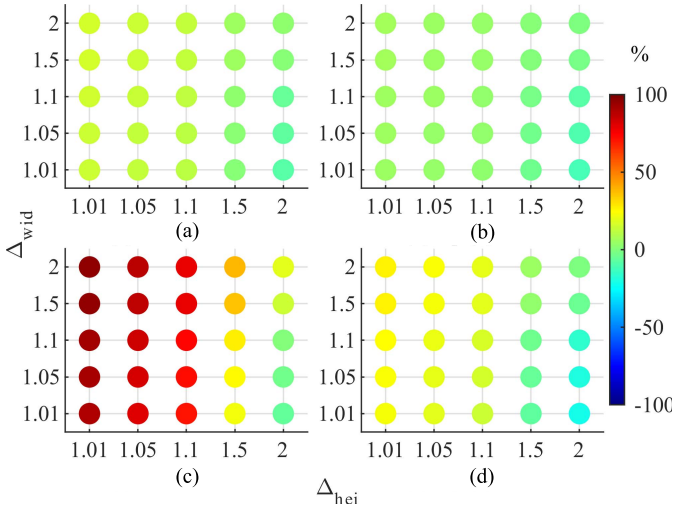

Fig. 9. Relative error% of proximity effect loss from (a) and (c) Ferreira's formula and (b) and (d) Ferreira's equation (4), compared with FEM results for different geometries; penetration ratios a/δ used are 1 and 2, respectively.

First, the relative error of Ferreira's formula and (5) for various geometries is shown in Fig. 9. It is obvious that (5) leads to much less error when Δ_{hei} is small, which proves that the conversion (4) can take the interaction between conductors into account. However, (5) still overestimates the proximity effect losses by about 20% when Δ_{hei} is 1.01. This is attributed to the fact that the interaction between conductors is not fully considered by (4).

Then, the relative error of the new equation with the geometry factor is compared with Nan's equation and Dowell's equation with various geometries and two penetration ratios are shown in Fig. 10. Compared with Dowell's model, the new equation and Nan's equation show better estimation over a wide range of geometry.

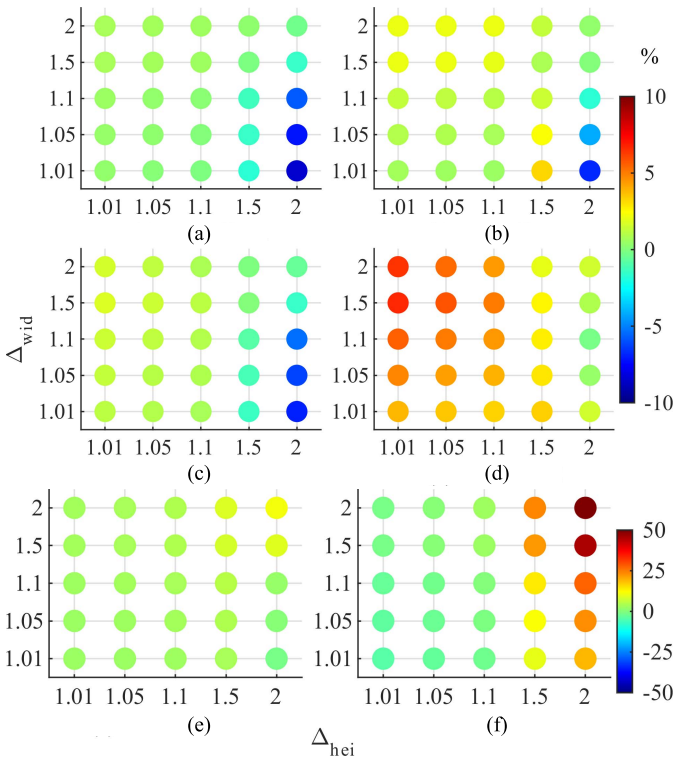

Fig. 10. (a) and (b) Relative error% of new equation, (c) and (d) Nan's equation, and (e) and (f) Dowell's model compared with FEM at different geometries; penetration ratios a/δ used are 1 and 2, respectively; (a)–(d) use upper color bar and (e) and (f) use bottom color bar.

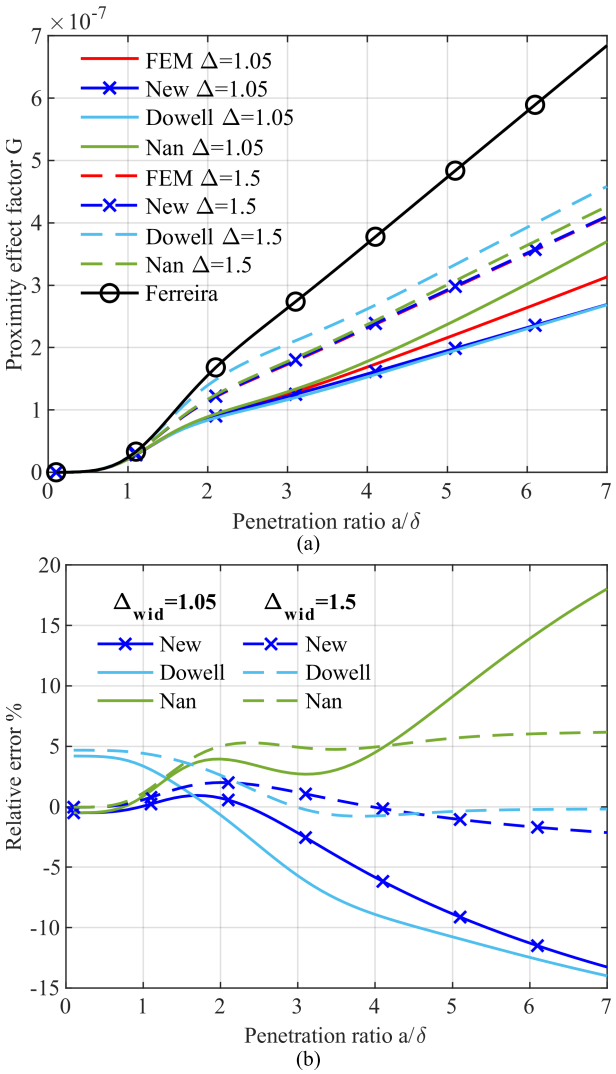

Fig. 11. (a) Proximity effect factors from FEM, Dowell's model, Ferreira's method, new equation, and Nan's equation, in the square cells where Δ is 1.05 and 1.5. (b) Relative errors of Dowell's model, new equation, and Nan's equation compared with FEM, in cells with the same $\Delta_{hei} = 1.1$ and varied $\Delta_{wid} = 1.05$ and 1.5.

As shown in Fig. 10(e) and (d), Dowell's model can provide accurate results when Δ_{hei} is small, which was shown in several references. For the new equation, estimations tend to underestimate the loss. The highest error always happens in cases with the highest Δ_{hei} and lowest Δ_{wid} and is around -10%. Because the interaction between the source and targeted conductor increases the magnetic field applied to the targeted conductor. Even using average field strength as H_0 in (1), it would underestimate the loss at a high penetration ratio, as Fig. 9(c) shown. However, situations like this are quite rare in layer windings, and the improved method is not considered in this article. According to Fig. 10(c) and (d), Nan's equation also provides results with less than 10% error and tends to overestimate the losses a bit.

Then, the proximity effect factor G from different methods in the square cells, whose Δ are 1.05 and 1.5, are shown in Fig. 11(a). First, results from Dowell's model and Ferreira's formula conform to other references [3], [4]. Then, the two improved methods show they can better cover more situations. When Δ is 1.05, the new equation underestimates losses at a high penetration ratio, and Nan's equation overestimates it. When Δ is 1.5, the new equation shows good results.

In Fig. 11(b), the relative errors of the new equation are shown, compared with FEM with constant Δ_{hei}, which is 1.1, and varied $\Delta_{wid} = 1.05$ and 1.5. One has $\Delta_{hei} > \Delta_{wid}$, another has $\Delta_{hei} < \Delta_{wid}$. The new equation and Nan's equation can give stable estimation with less than 5% error for the case with higher Δ_{wid}, dashed curves. In contrast, for the case with higher Δ_{hei}, solid curves, two improved equations lead to higher errors than dash curves. For the new equation, the larger errors can be attributed to the closer layers leading to a more significant interaction between layers and thus larger magnetic field changes. The new equation's curves present a slight overshoot in the small penetration ratio region. It is caused by the geometric factor λ, which is used to mitigate the impact of unideal fields. Dowell's model overestimates the proximity effect losses when the penetration ratio is smaller than 1.

In spite of the rectangular arrangement, the hexagonal arrangement is also widely used in windings. Therefore, the performance of the new equation is checked under several hexagonal arrangements. The model geometry is the same as in Fig. 2 in [15], and the boundary conditions use the same as in Fig. 6(c). The value Δ is decided by the ratio of the side length to the radius. Fig. 12 shows the relative error of different methods with different geometries. Compared with the results for rectangular arrangement, the new equation

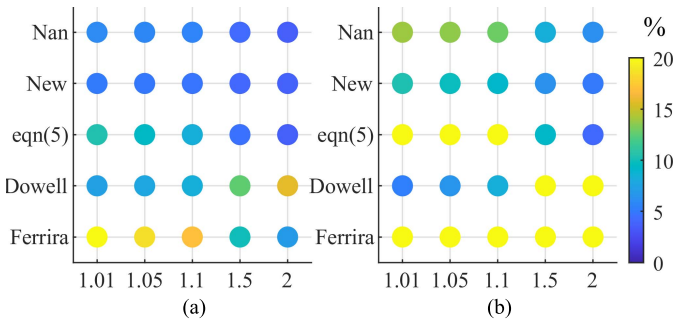

Fig. 12. Relative error% of external proximity effect loss from different methods compared with FEM in the hexagonal arrangements. The penetration ratios a/δ used are (a) 1 and (b) 2, respectively. For the value larger than 20%, the color is the same as the 20%.

has larger errors. It overestimates the losses by around 5% when the penetration ratio is 1. However, compared with other methods, it still performs more stable.

Based on these results, the new equation and Nan's equation can provide more accurate proximity effect loss estimation for round conductors in various geometries than classic methods. The new equation can still produce considerable error in small k cases, but these cases are rare in layer winding, and therefore are not investigated in more depth. The new equation already provides relatively good accuracy for most geometries and extreme cases with a low penetration ratio. For layer windings, if each layer produces the same amount of magneto-motivate force, the pth layer would suffer $(2p-1)^2$ times losses of the first layer from the proximity effect. Therefore, accurate proximity effect loss estimation is essential for ac winding loss calculation in multilayer windings.

C. Winding Losses Per Unit Length

Sections IV-A and IV-B compare losses from the skin and proximity effects independently. The impact of the method of image does not show up. In this section, results from simulation and several calculation methods for the losses per unit length in the same winding layout as measured sample is compared.

The results are shown in Fig. 13. There are several common phenomena in the two cases. Comparing the curves for the new equation with and without the method of images shows the impact of the implementation of the method of images. The method of images can effectively calculate the MMF over the boundary of layers and consider the impact of the gap between the core yoke and windings on winding losses. Results from Nan's method are close to that from the new equations without the method of images, because it does not consider the impact of gap, and it can result in similar accurate proximity effect losses as the new equation if the gap is not considered, as shown in Section IV-B. Dimitrakakis' method overestimates the losses in both cases. Because it assumes winding height is approximately equal to the window width. Therefore, the factors from curve fitting are not effective as in the targeted scenario.

In Fig. 13(a), the new approach and Dowell's model are closer to FEM results than other methods, and the first one is more accurate in the low penetration ratio region. In contrast,

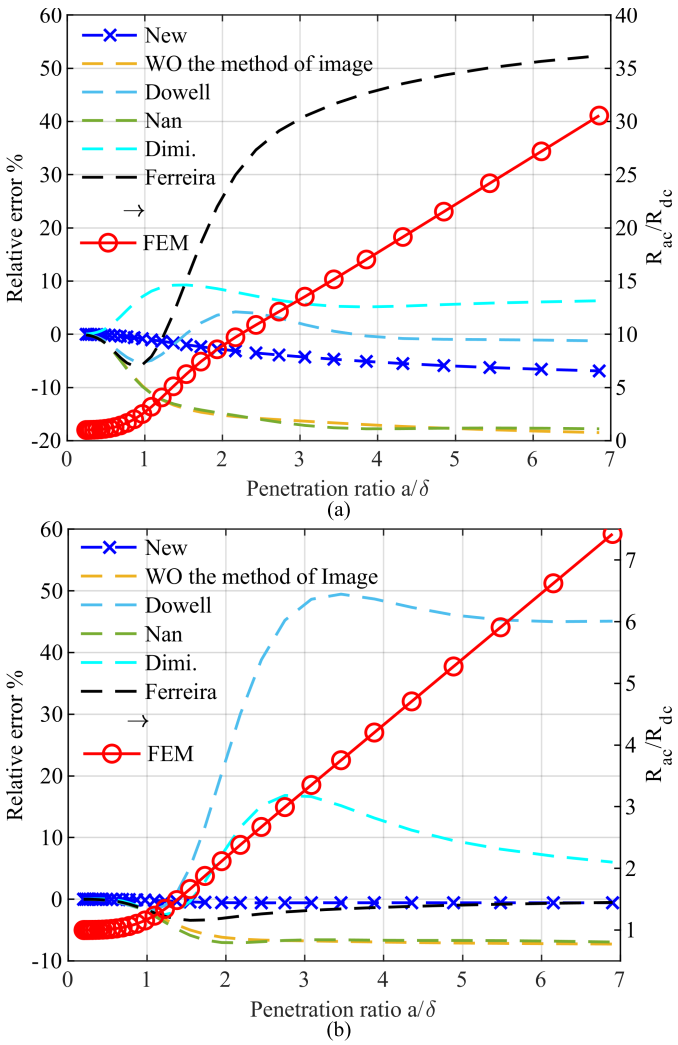

Fig. 13. Normalized ac resistance of FEM results and relative error of various methods compared with FEM, dash lines are relative error, and solid lines with circle are FEM result. (a) For DUT1. (b) For DUT2.

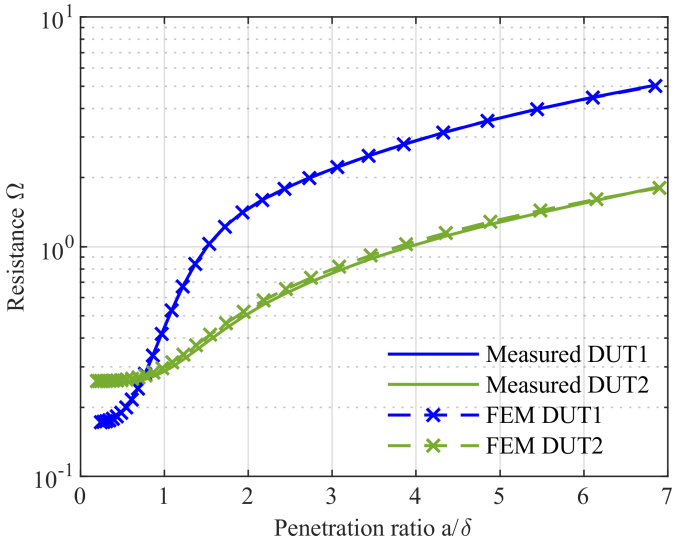

Fig. 14. Resistance from measurement and scaled FEM results for DUT1 and DUT2.

with an increasing penetration ratio, the error of the new approach increases. It is caused by the effectiveness of the

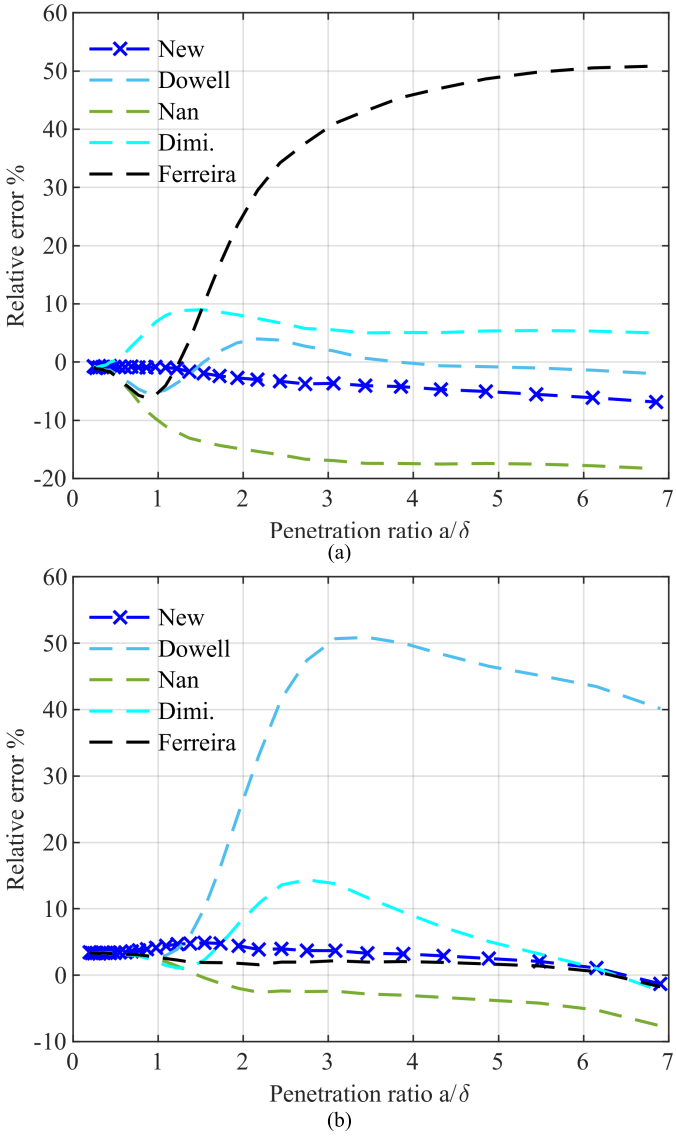

Fig. 15. Relative error of several analytical methods compared with the measured results. (a) For DUT1. (b) For DUT2.

geometric factor described in the previous section and the changing magnetic field in the window, which results in the error of the method of images. Fig. 13(b) shows the results of DUT2. The new approach's error is less than 5% over the whole curve and performs better than other methods. Ferreira's formula also gives an accurate result at a low porosity factor.

D. Measurement

The short circuit method was used to measure the ac resistance of transformer samples. The secondary winding was shorted, and the two connections of the primary winding were connected to an impedance analyzer. The measuring equipment used was an impedance analyzer Agilent 4294A.

The analytical layer winding loss calculation for sine waves is as follows.

1) Calculate the magnetic field applied on each layer.
2) Calculate each layer's losses per unit length inside a core window.
3) Scale the loss per unit length by the mean length of turns.

In Section IV-C, the loss per unit length is calculated. The ac resistances from the FEM simulation and the analytical methods are scaled with the mean turn length (MTL). Resistance of windings from the measurement and scaled FEM results are shown in Fig. 14. In both cases, results from measurement and scaled FEM results are almost overlapping. It indicates that 2-D FEM as a reference for comparison is effective.

Fig. 15(a) shows the relative error of different methods for DUT1. Dowell's model performs well and keeps the error between ±5%. The new approach shows comparable accuracy when the penetration ratio is lower than 5, but the error becomes larger with the increasing penetration ratio. Methods from Nan and Dimitrakakis result in larger errors, similar to the results in Fig. 13(b). For DUT2, the new approach and Ferreira's formula show highly accurate results for windings with a low porosity factor. Dowell's model overestimates the result substantially, and Nan's method still underestimates the results a bit. From the results of two different samples, the new approach shows its effectiveness for calculating losses of windings with gaps between the core and windings.

V. Conclusion

In this article, a new approach combining semi-empirical equations and the method of images is proposed for round conductor layer windings with un-gapped core. The neglection of interaction between conductors in Ferreira's formula is partly solved by converting constant MMF into a frequency-dependent uniform background magnetic field strength. The method of image is introduced to calculate the magnetic field, which could be applied to end-windings and cases with air gap by replacing air gap with a surface current density. The new method is compared with other analytical methods, FEM, and measurements. The results show that the winding loss calculation from the new method has less than 10% error for both high and low porosity factor cases, which can cover more cases than the classic method.

Appendix

According to [16], in Fig. 1(c), the magnetic field strength outside a conductor in polar coordinate is given by

$$H_{\mathrm{r}} = -H_0\left(1 + \frac{a^2 J_2(\zeta_2)}{r^2 J_0(\zeta_2)}\right)\sin(\varphi) \tag{19}$$

$$H_{\varphi} = -H_0\left(1 - \frac{a^2 J_2(\zeta_2)}{r^2 J_0(\zeta_2)}\right)\cos(\varphi). \tag{20}$$

Minus sign marks the direction of field. Then, convert back to Cartesian coordinate, y component is given as

$$H_y = -H_0\left(1 - \frac{a^2 J_2(\zeta_2)}{(x^2+y^2) J_0(\zeta_2)}\cos\left(2\arctan\left(\frac{y}{x}\right)\right)\right). \tag{21}$$

Integral over the vertical edge of cell is the same as the average field H_1 product length of edge. Relation between H_1 and H_0 is obtained

$$2\int_0^{\Delta_{\mathrm{hei}}a} H_y dy = -2H_0\left(\Delta_{\mathrm{hei}}a - \frac{\Delta_{\mathrm{hei}}a J_2(\zeta_2)}{(\Delta_{\mathrm{hei}}^2 + \Delta_{\mathrm{wid}}^2) J_0(\zeta_2)}\right) = -2\Delta_{\mathrm{hei}}a H_1. \tag{22}$$

ACKNOWLEDGMENT

This work was supported by the China Scholarship Council under Grant 202007720032.

REFERENCES

[1] P. Dowell, "Effects of eddy currents in transformer windings," *Proc. Inst. Electr. Eng.*, vol. 113, no. 8, p. 1387, 1966.
[2] J. A. Ferreira, "Improved analytical modeling of conductive losses in magnetic components," *IEEE Trans. Power Electron.*, vol. 9, no. 1, pp. 127–131, Jan. 1994.
[3] M. Kaymak, Z. Shen, and R. W. De Doncker, "Comparison of analytical methods for calculating the AC resistance and leakage inductance of medium-frequency transformers," in *Proc. IEEE 17th Workshop Control Modeling Power Electron. (COMPEL)*, Jun. 2016, pp. 1–8.
[4] G. S. Dimitrakakis and E. C. Tatakis, "Investigation of high frequency effects on layered coils," in *Proc. 13th Int. Power Electron. Motion Control Conf.*, Sep. 2008, pp. 1301–1308.
[5] A. Reatti and M. K. Kazimierczuk, "Comparison of various methods for calculating the AC resistance of inductors," *IEEE Trans. Magn.*, vol. 38, no. 3, pp. 1512–1518, May 2002.
[6] X. Nan and C. R. Sullivan, "An improved calculation of proximity-effect loss in high-frequency windings of round conductors," in *Proc. IEEE Annu. Power Electron. Spec. Conf. (PESC Record)*, vol. 2, Jun. 2003, pp. 853–860.
[7] D. Whitman and M. K. Kazimierczuk, "An analytical correction to Dowell's equation for inductor and transformer winding losses using cylindrical coordinates," *IEEE Trans. Power Electron.*, vol. 34, no. 11, pp. 10425–10432, Nov. 2019.
[8] X. Nan and C. R. Sullivan, "Simplified high-accuracy calculation of eddy-current loss in round-wire windings," in *Proc. IEEE Annu. Power Electron. Spec. Conf. (PESC Record)*, vol. 2, Jun. 2004, pp. 873–879.
[9] G. S. Dimitrakakis, E. C. Tatakis, and E. J. Rikos, "A semiempirical model to determine HF copper losses in magnetic components with nonlayered coils," *IEEE Trans. Power Electron.*, vol. 23, no. 6, pp. 2719–2728, Nov. 2008.
[10] M. Bartoli, N. Noferi, A. Reatti, and M. K. Kazimierczuk, "Modelling winding losses in high-frequency power inductors," *J. Circuits, Syst. Comput.*, vol. 5, no. 4, pp. 607–626, Dec. 1995.
[11] J. Muhlethaler, J. W. Kolar, and A. Ecklebe, "Loss modeling of inductive components employed in power electronic systems," in *Proc. 8th Int. Conf. Power Electron. (ECCE Asia)*, May 2011, pp. 945–952.
[12] M. A. Bahmani, T. Thiringer, and H. Ortega, "An accurate pseudoempirical model of winding loss calculation in HF foil and round conductors in switchmode magnetics," *IEEE Trans. Power Electron.*, vol. 29, no. 8, pp. 4231–4246, Aug. 2014.
[13] X. Nan and C. R. Sullivan, "An equivalent complex permeability model for Litz-wire windings," *IEEE Trans. Ind. Appl.*, vol. 45, no. 2, pp. 854–860, Mar./Apr. 2009.
[14] H. Igarashi, "Semi-analytical approach for finite-element analysis of multi-turn coil considering skin and proximity effects," *IEEE Trans. Magn.*, vol. 53, no. 1, pp. 1–7, Jan. 2017.
[15] D. C. Meeker, "An improved continuum skin and proximity effect model for hexagonally packed wires," *J. Comput. Appl. Math.*, vol. 236, no. 18, pp. 4635–4644, Dec. 2012.
[16] J. Lammeraner and M. Štafl, *Eddy Currents*. Boca Raton, FL, USA: CRC Press, 1966.
[17] A. D. Podoltsev, I. N. Kucheryavaya, and B. B. Lebedev, "Analysis of effective resistance and eddy-current losses in multiturn winding of high-frequency magnetic components," *IEEE Trans. Magn.*, vol. 39, no. 1, pp. 539–548, Jan. 2003.
[18] C. Carretero, J. Acero, and R. Alonso, "TM-TE decomposition of power losses in multi-stranded Litz-wires used in electronic devices," *Prog. Electromagn. Res.*, vol. 123, pp. 83–103, 2012.
[19] M. Lambert, F. Sirois, M. Martinez-Duro, and J. Mahseredjian, "Analytical calculation of leakage inductance for low-frequency transformer modeling," *IEEE Trans. Power Del.*, vol. 28, no. 1, pp. 507–515, Jan. 2013.
[20] L. R. Stoll, *The Analysis of Eddy Currents*. Oxford, U.K.: Clarendon, 1974.

Tianming Luo (Graduate Student Member, IEEE) was born in Jinan, China, in 1993. He received the B.E. degree in electrical engineering and automation from Chongqing University, Chongqing, China, in 2015, and the M.Sc. degree from the China Electric Power Research Institute, Beijing, China, in 2018. He is currently pursuing the Ph.D. degree with the DC System, Energy Conversion and Storage Group, Technical University of Delft, Delft, The Netherlands.

His current research interests include multiphysics model of medium-frequency power transformer and insulation performance under medium frequency.

Mohamad Ghaffarian Niasar was born in Tehran, Iran, in 1984. He received the M.Sc. degree from the Sharif University of Technology, Tehran, in 2008, and the Ph.D. degree in electrical engineering from the Royal Institute of Technology (KTH), Stockholm, Sweden, in 2015.

He is currently an Assistant Professor with the DC System, Energy Conversion and Storage Group, Technical University of Delft, Delft, The Netherlands. His current research interests include aging of insulation material, HVdc insulation system, high-frequency power transformers, and multiphysics modeling of power components.

Peter Vaessen (Member, IEEE) was born in Maasbree, The Netherlands, in 1960. He received the M.Sc. degree (cum laude) in electrical power engineering from Eindhoven Technical University, Eindhoven, The Netherlands, in 1985.

In 1985, he joined KEMA (now a CESI brand), The Netherlands. In his 35-year career, he held research positions in the fields of large power transformers and high-voltage measurement and testing. He has 25 years of experience in (U)HVdc technology and T and D grids with high shares of renewables. He is an Innovation Manager with the KEMA Laboratories and the Chairman of the European Distributed Energy Resources Laboratories Association (DERlab), as well as a member of several national and international working groups. Since 2017, he is a Part-Time Professor of hybrid transmission systems with TU Delft, Delft, The Netherlands, where he teaches high-voltage technology and HVdc.